A Computational Study of a New Dual Throat Fluidic Thrust Vectoring Nozzle Concept

Karen A. Deere[*], Bobby L. Berrier[†], Jeffrey D. Flamm[‡]
Aerodynamics, Aerothermodynamics, and Acoustics Competency
NASA Langley Research Center, Hampton, VA, 23681-0001

Stuart K. Johnson[§]
Aerospace Systems Concepts & Analysis Competency
NASA Langley Research Center, Hampton, VA, 23681-0001

A computational investigation of a two-dimensional nozzle was completed to assess the use of fluidic injection to manipulate flow separation and cause thrust vectoring of the primary jet thrust. The nozzle was designed with a recessed cavity to enhance the throat shifting method of fluidic thrust vectoring. Several design cycles with the structured-grid, computational fluid dynamics code PAB3D and with experiments in the NASA Langley Research Center Jet Exit Test Facility have been completed to guide the nozzle design and analyze performance. This paper presents computational results on potential design improvements for best experimental configuration tested to date. Nozzle design variables included cavity divergence angle, cavity convergence angle and upstream throat height. Pulsed fluidic injection was also investigated for its ability to decrease mass flow requirements. Internal nozzle performance (wind-off conditions) and thrust vector angles were computed for several configurations over a range of nozzle pressure ratios from 2 to 7, with the fluidic injection flow rate equal to 3 percent of the primary flow rate. Computational results indicate that increasing cavity divergence angle beyond 10° is detrimental to thrust vectoring efficiency, while increasing cavity convergence angle from 20° to 30° improves thrust vectoring efficiency at nozzle pressure ratios greater than 2, albeit at the expense of discharge coefficient. Pulsed injection was no more efficient than steady injection for the Dual Throat Nozzle concept.

Nomenclature

$C_{d,p}$	=	system discharge coefficient, $(w_p + w_s)/w_{i,p}$
$C_{fg,sys}$	=	system thrust ratio, $F_r/(F_{i,p} + F_{i,s})$
d	=	cavity depth
DTN	=	dual throat nozzle
F_A	=	axial force
$F_{i,p}$	=	ideal isentropic thrust of primary flow
$F_{i,s}$	=	ideal isentropic thrust of fluidic injection flow
F_N	=	normal force
F_r	=	resultant force
F_S	=	side force
h_{ut}	=	height at upstream minimum area
h_{dt}	=	height at downstream minimum area
JETF	=	Jet Exit Test Facility
k	=	turbulent kinetic energy
l	=	cavity length
LCA	=	lower cavity angles
M	=	freestream Mach number

[*] Aerospace Engineer, Configuration Aerodynamics Branch, MS 499, and AIAA Senior Member.
[†] Aerospace Engineer, Configuration Aerodynamics Branch, MS 499, and AIAA Fellow.
[‡] Aerospace Engineer, Configuration Aerodynamics Branch, MS 499, and AIAA Senior Member.
[§] Aerospace Engineer, Advanced Aircraft Systems Branch, MS 411.

NPR	=	nozzle pressure ratio, $p_{t,j}/p_\infty$
NPR_D	=	design nozzle pressure ratio
p	=	surface static pressure
P_o	=	total pressure
$p_{t,j}$	=	primary flow total pressure
p_∞	=	freestream static pressure
$w_{i,p}$	=	ideal primary weight flow
$w_{i,s}$	=	ideal fluidic injection weight flow
w_p	=	actual primary weight flow
w_s	=	actual fluidic injection weight flow
x	=	axial distance
x_1	=	length of cavity divergence section
x_2	=	length of cavity convergence section
y^+	=	nondimensional first cell height
z	=	distance above or below nozzle centerline
δ_p	=	pitch thrust-vector angle, $\tan^{-1}(F_N/F_A)$
δ_y	=	yaw thrust-vector angle, $\tan^{-1}(F_S/F_A)$
ε	=	turbulent energy dissipation rate
η	=	thrust-vectoring efficiency, $\delta_p/[w_s/(w_s+w_p)*100]$
θ_1	=	cavity divergence angle
θ_2	=	cavity convergence angle

I.   Introduction

The Aerospace Vehicle Systems Technology Office at NASA Langley Research Center (LaRC) has the objective to revolutionize the aircraft of the future. The vision includes sleek personal air vehicles and supersonic business jets that fly more birdlike than current airplanes which have a fuselage tube, wings and tails, and are maneuvered with conventional control surfaces. Some of the benefits of a revolutionary design include noise reduction, improved ride quality, increased passenger and aircraft safety, improved maneuverability, improved survivability, decreased landing speeds, and adaptability to short runways. A suite of innovative control effectors are needed to manipulate the more seamless aircraft of the future, in which conventional control surfaces that contain breaks, gaps and discontinuities in the airplane 'skin' are eliminated. Fluidic thrust vectoring is a prime control effector in the suite of controls that are needed to maneuver the next generation aircraft, many of which conceptually have no vertical tail. Fluidic thrust vectoring continues to work at low dynamic pressures, where other candidate control technologies fail, making it a valuable control effector at the edges of the flight envelope. Further, fluidic thrust vectoring and fluidic throat area control allow for structurally fixed nozzles that will weigh less than mechanical thrust vectoring nozzles that require actuated hardware to force the exhaust flow off axis or to vary throat area.

Fluidic thrust vectoring is the manipulation or control of the exhaust flow from a jet engine by the use of a secondary air source, which is typically bleed air from the engine compressor or fan. Three primary mechanisms of fluidic thrust vectoring that have been studied over the last 10 years are shock-vector control, throat shifting, and counterflow[1-13]. These techniques can be used to vector the exhaust flow in the pitch direction with the magnitude measured by pitch vector angle δ_p or in the yaw direction with the magnitude measured by yaw vector angle δ_y. A means of comparing the thrust vector angles of different fluidic injection techniques or configurations is thrust vectoring efficiency η, which is defined as the thrust vector angle in degrees (δ_p or δ_y), normalized by the percent of secondary fluidic injection. Other parameters for evaluating nozzle performance of thrust vectoring nozzles are system thrust ratio ($C_{fg,sys}$) and system discharge coefficient ($C_{d,p}$).

The shock-vector control method[1-6] is a thrust-vectoring method, which introduces fluidic injection into the supersonic flow downstream of the nozzle throat. Substantial thrust vectoring efficiencies are generated at the expense of system thrust ratio as the flow is robustly turned through oblique shocks in the nozzle. Throat shifting methods[7-10] utilize fluidic injection at the nozzle throat to turn the subsonic flow ahead of the nozzle throat; subsonic flow turning incurs lower losses than supersonic flow turning. Therefore, throat shifting methods typically achieve higher system thrust ratios than shock-vector control methods, which operate best at off-design conditions and have losses due to shocks in the nozzle. Although throat shifting methods are currently improving, most thrust vector angles reported to date require up to 6% engine bleed to obtain reasonable amounts of thrust vectoring. The counterflow method[11-12] (suction in a secondary duct near throat) provides large thrust vector angles with little

secondary flow requirements, but issues such as suction supply source, hysteresis effects, and airframe integration need to be addressed. Since there is no straightforward manner to compare an applied suction approach to the fluidic injection techniques, the reader is directed to references 11 and 12 for further details on the counterflow method.

Researchers at NASA LaRC have designed and are exploring a new fluidic thrust vectoring technique that achieves larger thrust vectoring efficiencies than the traditional throat shifting method, without compromising system thrust ratio.   This new nozzle design provides thrust vectoring capability by controlling separation and maximizing pressure differentials in a recessed cavity, which is created between two minimum areas, or throats (Fig. 1). Hence, the nozzle has been denoted as the Dual Throat Nozzle. Experimentally, the Dual Throat Nozzle achieved an impressive thrust vectoring efficiency of $\eta = 7.7°$/%-injection at a nozzle pressure ratio of NPR=2 and obtained a system thrust ratio of $C_{fg,sys}$=0.963 at this vectoring condition, (less than a 1% loss of thrust due to secondary injection)[14]. Even at an NPR=5 where traditional throat shifting methods have difficulty maintaining high thrust vectoring efficiencies, the Dual Throat Nozzle achieved an experimental thrust vectoring efficiency of η=5.8°/%-injection and maintained a system thrust ratio of $C_{fg,sys}$=0.962, (0.2% loss of thrust due to secondary injection). For comparison, an advanced traditional throat shifting nozzle design found in open literature[9] achieved thrust vectoring efficiencies up to $\eta = 3.9°$/%-injection at an off-design condition of NPR=2 and $\eta = 2°$/%-injection at the design condition of NPR=5.5. The 2.1% ($C_{fg,sys}$=0.924) and 1.7% ($C_{fg,sys}$=0.956) reductions in thrust efficiency compared to the non-thrust vectoring cases for NPR=2 and NPR=5.5, respectively, were termed small losses in reference 9. The best shock vector control nozzle from NASA LaRC data[13] achieved a thrust vectoring efficiency of η=4.5°/%-injection at an off-design condition of NPR=3, but incurred a large thrust efficiency penalty ($C_{fg,sys}$=0.89). At NPR=5, several shock vector control configurations from NASA LaRC data[13] achieved thrust vectoring efficiencies near η=2.6°/%-injection with system thrust ratios in the range of $C_{fg,sys}$=0.89-0.95. Nozzle pressure ratios around 2 to 3 occur at low-speed and take-off and landing conditions, while the design condition (NPR=5.5 for one nozzle discussed above) would be typical of high subsonic or low supersonic operation where mild maneuvering might be necessary.

The structured-grid, computational fluid dynamics (CFD) code PAB3D was used to aid the design of the two-dimensional (2D), fluidic thrust vectoring, Dual Throat Nozzle[10]; the concept was validated experimentally[14] in the Jet Exit Test Facility (JETF) at the NASA LaRC. Several CFD design and experimental validation cycles were completed. In the current investigation, 2D PAB3D simulations were conducted on the best experimental configuration tested to date in order to quickly screen several geometric parameters that could further impact thrust vectoring efficiency and nozzle performance. The nozzle geometric design variables (shown in Fig. 2) discussed herein include cavity divergence angle (θ_1), cavity convergence angle (θ_2), and upstream minimum height (h_{ut}). Several configurations exploring these variables were simulated at nozzle pressure ratios from 2 to 7 with either no fluidic injection, or with a steady secondary fluidic injection rate equal to 3 percent of the primary flow rate at a static freestream Mach number. Pulsed fluidic injection was investigated as a means for maintaining thrust vector angles while decreasing secondary weight flow requirements, which would reduce the impact of bleeding air from the engine for fluidic injection. Details of the experimental configuration and data are included in the reference 14 companion paper.

II.   Computational Method

The CFD code PAB3D was used to predict thrust vectoring efficiency and nozzle performance of the 2D, fluidic thrust vectoring Dual Throat Nozzle. PAB3D was chosen for this work because it was originally developed as a propulsion (internal flow) code and now has been well tested and documented for predicting complex flow features in aeropropulsive, as well as aerodynamic configurations[15-25].

PAB3D requires a structured-mesh computational domain and the multiblock[16] feature allows the domain to be partitioned into sections, which is critical for modeling complex configurations and for efficiently running the parallel version of PAB3D. The implicit, finite-volume flow solver represents the three-dimensional (3D), unsteady Reynolds-averaged Navier-Stokes (URANS) equations. Several advanced turbulence models[26-29] are available for closure of the URANS equations. The desire to simulate pulsed fluidic injection with an unsteady injection boundary condition and to capture the unsteady flow features in the Dual Throat Nozzle, as well as other requests within NASA and the US aerospace industry, prompted the upgrade of PAB3D to a second order time-accurate CFD code with time-varying boundary conditions[30-31].

A. Governing Equations

The governing equations, which include the conservation equations for mass, momentum, and energy, along with the equation of state, are written in generalized coordinates and in conservative form. In an effort to decrease

computational resources, the simplified, thin-layer Navier-Stokes equations are implemented into PAB3D. This approximation neglects derivatives in the viscous terms in the streamwise and parallel directions to the surface, since they are typically negligible in comparison to the derivatives normal to the surface. The flow solver was written with three numerical schemes: the flux vector-splitting scheme of van Leer[32], the flux difference-splitting scheme of Roe, and a modified Roe scheme primarily used for space marching solutions. These schemes implement the finite volume principle to balance the fluxes across grid cells and the upwind biased scheme of van Leer or Roe to determine fluxes at the cell interfaces. Only the inviscid terms of the flux vectors are split and upwind differenced, while the diffusion terms of the Navier-Stokes equations are central differenced. Several limiters are available for numerical stability. Recent enhancement of the time advancement formulation improves time accuracy with a dual time stepping or physical time stepping sub-iteration scheme[30]. Extensive details of PAB3D are found in references 15 through 30 and code documentation is located at http://www.asm-usa.com/software/PAB3D/PAB3D-Doc.html.

B. Turbulence Modeling

PAB3D offers several advanced turbulence models[26-29] for closure of the URANS equations. The 2-equation k-ε turbulence model, often used to simulate complex viscous flow features, may be selected with an eddy viscosity hypothesis implementation or with an Explicit Algebraic Reynolds Stress Model (ARSM)[27-28]. The eddy viscosity hypothesis is based on a linear relationship between stress and strain that can produce inaccurate normal Reynolds stress differences for some flow fields. In an effort to capture any anisotropic flow features that may be present in the flow field, ARSMs are based on the theory that the Reynolds stresses are related to k, ε, and the mean velocity gradients. The Girimaji ARSM used in the current work models a pressure/strain relationship between the turbulent Reynolds stresses and the mean velocity field[27].

The pair of coupled transport equations, turbulent kinetic energy (k) and turbulent energy dissipation rate (ε), are written in conservative form and can be uncoupled from the Navier-Stokes equations and from each other to decrease computational requirements. Since the k-ε turbulence model has a singularity at solid surfaces, either a damping function or a wall function must be implemented to adjust the turbulent energy dissipation rate (ε) at solid surfaces. The grid in the boundary layer at wall surfaces must be well defined with a law-of-the-wall coordinate (y^+) of 2 or less, for adequate modeling of the boundary layer flow[20]. The restriction on y^+ may be relaxed to 50 if a wall function approach is selected for the computation. However, it is customary to restrict the use of a wall function to attached flow only, which typically only occurs in nozzle flows at NPR≥NPR$_D$. Exhaust nozzles utilizing fluidic injection generally experience regions of separated flow, such that the wall function is not appropriate. Likewise, all nozzles at overexpanded conditions (NPR<NPR$_D$) contain regions of flow separation.

C. Computational Solution

For the current work, the URANS equations were solved with a k-ε turbulence model invoking the Girimaji nonlinear stress model[27-28]. A modified Jones and Launder form of the damping function[33] was implemented in the wall-bounded blocks to treat the singularity at the wall and a high Reynolds number model was selected for the freestream blocks. Solutions are third order accurate in space. The dual time sub-iteration scheme was used for the time advancement formulation, to improve time accuracy to second order[30]. The van Leer flux vector-splitting scheme[32], the Roe flux difference-splitting scheme and the Spekereijse-Venkate limiter were all implemented in each block.

D. Boundary Conditions

The PAB3D code has many options for defining the conditions of the inflow, outflow, freestream, wall, symmetry and centerline boundaries. Additionally, several unsteady boundary conditions[31] were implemented into the PAB3D flow solver at the request of the authors to research the best application for simulating pulsed secondary air injection. Either a total pressure or velocity pulsing boundary condition may be selected, which may vary as a function of a cosine or square waveform. Pulsing function variables include amplitude, frequency, phase and duty cycle.

For this study, Riemann invariants along the characteristics were implemented along the lateral and in-flow freestream boundaries. At the downstream far field boundary, a subsonic, constant pressure outflow boundary condition was used, which automatically switches to first order extrapolation if the flow is supersonic. The primary nozzle flow and the fluidic injection flow were specified with a fixed total-temperature and total-pressure boundary condition. A no-slip, adiabatic wall boundary condition was implemented on nozzle surfaces to obtain viscous solutions. For these 2D simulations, a symmetry boundary condition was used in the third dimension. Although

several unsteady boundary conditions were investigated for the pulsed injection simulations, the total pressure square wave boundary condition was used for most of the work.

E. Performance Calculations and Post Processing

Nozzle performance and thrust vector angles were computed with the PAB3D post processor code, POST. Likewise, pressure distributions and flow contours were extracted with POST. The POST software package documentation is located at http://www.asm-usa.com/software/PAB3D/doc/post/. TECPLOT was used for plotting all data.

F. Nozzle Geometry

Sketches of the Dual Throat Nozzle (DTN) concept are shown in Figs. 1 and 2; a photograph of the experimental model mounted on the dual-flow propulsion simulation system in JETF can be found in Fig. 2 of the experimental companion paper[14]. The DTN geometry is intended to enhance the thrust vectoring capability of the throat shifting method by manipulating flow separation in a recessed cavity. The recessed cavity section was located between upstream and downstream minimum areas and fluidic injection was introduced at the upstream minimum area location (Fig. 1). The nozzle geometric design variables (shown in Fig. 2) discussed herein include cavity divergence angle (θ_1), cavity convergence angle (θ_2), and upstream minimum height (h_{ut}).

In the current investigation, the best experimental nozzle performer to date (herein denoted as configuration 1, listed in Table 1) was used to investigate geometric parameters that could further impact thrust vectoring efficiency and nozzle performance. Configuration 1 was used to computationally investigate the effects of cavity divergence angle and cavity convergence angle. Experimentally, fluidic injection was implemented through a row of injection holes. In the 2D computational domain with symmetry boundary conditions for the third dimension, the injection opening and plenum would be more representative of a slot in three dimensions.

Configuration 2 (Table 1) was used to investigate variations on the upstream throat height. This configuration was chosen after the investigation of the effects of cavity angles on thrust vectoring and nozzle performance.

Configuration 3 (Table 1) was used to investigate the effects of pulsed fluidic injection on thrust vectoring efficiency and nozzle performance. Although the experimental nozzle was designed with $h_{ut}=h_{dt}=1.15$ inches, the actual assembled hardware and therefore, the computational domain, had $h_{ut}=h_{dt}=1.18$ inches.

Configuration	θ_1, °	θ_2, °	h_{ut}, in.	h_{dt}, in.	l, in.	Investigate Effects of:
1	10	20	1.15	1.15	3	Cavity Angles
2	10	30	variable	1.15	3	Upstream Throat Height
3	10	20	1.18	1.18	1	Pulsed injection

Table 1. Geometry definitions of the configurations used for the computational investigation.

G. Computational Domain

Two-dimensional meshes were used in order to quickly evaluate a multitude of geometric parameters. For the cavity angle and upstream throat height study, the computational domain was defined with 30 blocks; 24 blocks inside the nozzle, 1 block defining the fluidic injection plenum, and 5 blocks defining the freestream domain. The far field was located 15 cavity lengths downstream and 2 cavity lengths upstream of the nozzle exit. The upper and lower lateral far field boundaries were located 25 cavity lengths above and below the nozzle. The first grid height in the boundary layer was defined for $y^+=0.5$ on the fine mesh spacing for adequate modeling of the boundary layer flow and its interaction with secondary flow injection. The fluidic injection slot was 0.02 inches wide.

For the pulsed injection study, the computational domain representing the experimental configuration was modeled with 11 blocks: 4 blocks inside the nozzle, 2 blocks defining the fluidic injection plenum, and 5 blocks defining the freestream domain. The far field was located 75 cavity lengths downstream and 10 cavity lengths upstream of the nozzle exit. The upper and lower lateral far field boundaries were located 75 cavity lengths above and below the nozzle. The first grid height in the boundary layer was defined for $y^+=0.5$ on the fine mesh spacing for adequate modeling of the boundary layer flow. The fluidic injection slot was 0.01 inches wide.

H. Pulsed Injection

For the pulsed fluidic injection simulations, several oscillating boundary conditions were investigated. Pulsed injection was initially modeled with a cosine wave, but then represented with a square wave to more realistically simulate an on/off injection modulator. Simulations shown here were predicted at NPR=4, with a time-averaged injection rate of 5 percent of the primary flow. Flow condition variables for the pulsed injection study included

frequency range (2 to 100 kHz), amplitude (.25, 0.5, and 0.75) and time on/time off duty cycle (25%, 50% and 75%). The amplitude specified the maximum and minimum total pressures, such that a 0.25 amplitude had maximum and minimum pressures 25% higher and lower than steady state total pressure. The duty cycle for the square wave boundary condition specified the duration (in percent) of peak total pressure during one period.

III.   Results

The CFD code PAB3D was used to guide the initial design of the 2D, fluidic thrust vectoring, Dual Throat Nozzle concept[10]. The first experimental validation of this concept was completed in the NASA LaRC JETF and is reported in reference 14. The current paper reports PAB3D computational results that were used to investigate further nozzle design changes for improving thrust vectoring and nozzle performance. For example, the effects of cavity divergence angle and cavity convergence angle were tested experimentally for a configuration with a cavity length of 1 inch. Additionally, the effect of cavity length was also investigated experimentally, which indicated that better thrust vectoring efficiency was achieved with a 3-inch cavity length. However, without the necessary hardware available to test the effect of cavity divergence angle and convergence angle on the longer (and better performing) cavity length nozzle, CFD played an essential role for confirming the effects of these variables on the longer cavity length configuration.

All experimental data acquired to date on the DTN have been at static freestream conditions. Likewise, the computational solutions were simulated with a static freestream, although a small convective Mach number of M=0.01 was used for computational stability. The effects of cavity convergence and divergence angles on nozzle performance and thrust vectoring efficiency were predicted at NPRs=2, 4, and 7 with 3% injection, while effect of throat height was simulated at NPR=4 with 3% injection.

A. Experimental and Computational Comparisons

Simulations of configuration 1 operating at NPRs 2, 4 and 7 were computed with no injection and 3% injection. The comparison of predicted results with experimental data for discharge coefficient, system thrust ratio, thrust vectoring efficiency and thrust vector angle are shown in Fig. 3 and a comparison of internal static pressure distributions at NPR=2 is shown in Fig. 4.

Computational results indicated a 7% decrease in discharge coefficient while thrust vectoring with 3% injection (Fig. 3(d)), relative to the no thrust vectoring (no injection) case (Fig. 3(a)), while experimental data validated a 6% decrease over the range of NPR tested. There was a smaller impact on system thrust ratio for thrust vectoring cases, relative to the no injection cases. Although the magnitude was not predicted, PAB3D did accurately predict the larger penalty in system thrust ratio for fluidic thrust vectoring at NPR=2 relative to no injection, than at NPR>2. Thrust vectoring efficiency was predicted well, within 0.15°/%-injection, at NPR>2. Computational results indicated less thrust vectoring at NPR=2 than demonstrated experimentally in the JETF, which indicates more flow separation and a larger pressure differential with the 3D experimental configuration, than predicted with a 2D simulation (Fig. 3(f)). Figure 4 shows that upper-wall pressures were predicted fairly well at NPR=2, with slightly more expansion around the upstream throat (0<x<0.4 inches) and higher pressures on the cavity convergent section (2<x<3 inches). Lower-wall pressures in the convergent cavity section were higher than experiment, resulting in a smaller pressure differential and thus, a smaller thrust vector angle than experiment.

Even though an advanced turbulence model with nonlinear Reynolds stress modeling was used for these simulations, all turbulence models have some level of difficulty accurately predicting separation. The fluidic thrust vectoring, Dual-Throat Nozzle concept relies on separation in the recessed cavity to create a large pressure differential between the upper and lower walls to vector the primary jet thrust. Therefore, it was not surprising that the magnitude of thrust vector angle, discharge coefficient and system thrust ratios were not predicted exactly. The predicted discharge coefficient was up to 2.3% lower and system thrust ratio was up to 1.4% lower than experiment. The lower discharge coefficient and system thrust ratios relative to experiment suggests that computational results predicted a larger total pressure loss, at the nozzle exit, due to separated turbulent flow in the lower cavity. A band of low total pressure flow can be observed exiting the nozzle near the lower lip in Figure 5. The other differences that may result in minor discrepancies between experimental and computational data include differences between the as-built experimental hardware and the modeled computational domain. Experimentally, the nozzle was a 3D rectangular configuration with a row of injection holes, while the 2D computational domain mimicked an injection slot.

After reviewing Fig. 3, it is important to remember that the computational simulations were used to guide the design of the DTN and not to provide absolute magnitudes of nozzle performance. Although PAB3D did not predict the absolute magnitudes of configuration 1 at NPRs 2, 4, and 7 with no injection or with 3% injection, the trends of

thrust vectoring efficiency, discharge coefficient and system thrust ratio were predicted well. Predicting the trends in performance makes PAB3D an invaluable tool for screening a multitude of geometric and flow condition variables, in an effort to guide the design of the DTN. Promising configurations and design features can then be validated experimentally in the NASA LaRC JETF.

B. Effect of Cavity Divergence Angle

The predicted effects of cavity divergence angle on thrust vectoring efficiency, discharge coefficient and system thrust ratio are shown in Fig. 6. Increasing cavity divergence angle had a negative impact on system thrust ratio $C_{fg,sys}$ and thrust vector angle δ_p for all NPR. Discharge coefficient also decreased very slightly with increased cavity divergence angle.

The flow was mostly separated from both the upper and lower cavity walls at cavity divergence angles greater than 10°, resulting in large losses of thrust vectoring efficiency for $\theta_l > 10°$ at all NPR. The increased flow separation on the nozzle upper wall that results in a loss of thrust vectoring efficiency is evident in the cavity wall pressures shown in Fig. 7 for NPR=4, which is representative of all NPRs studied. Although, cavity divergence angle had little impact on the lower cavity wall pressures, the pressure differential between the upper and lower cavity walls was severely degraded by increased flow separation on the upper cavity divergent wall as indicated by pressure distributions that are more flat in nature than the $\theta_l = 10°$ case. The separated flow from the upper cavity wall was also apparent in the Mach contours shown in Fig. 8.

C. Effect of Cavity Convergence Angle

The predicted effects of cavity convergence angle on thrust vectoring efficiency, discharge coefficient and system thrust ratio are shown in Fig. 9. For NPRs 4 and 7, thrust vectoring performance improved when cavity convergence angle was increased from 20° to 30°, and then decreased slightly as convergence angle was increased to 40°. However, an undesirable consequence of increasing cavity convergence angle was a decrease in discharge coefficient ($C_{d,p}$) at all NPRs, which can be detrimental to engine operating stability or can increase the size of the nozzle required for a given airflow.

Unlike cavity divergence angle, cavity convergence angle does impact lower wall cavity pressures as indicated in Figure 10. Increasing cavity convergence angle increases lower wall cavity pressures, which could act to decrease thrust vector angle unless upper wall pressures are also increased by the same magnitude or more. Improved thrust vectoring with the 30° convergence angle resulted from two factors; elimination of the flow expansion after the sonic throat and before the strong shock ($0.4 < x < 1$), and increased pressures on the upper wall in the convergence section of the cavity ($2.2 < x < 3$). Both of these results increased the pressure difference between the upper and lower nozzle surfaces, resulting in better thrust vectoring performance than with the 20° convergence angle. Although the pressures on the upper wall were increased further with the 40° convergence angle, the pressures on the lower surface were also increased and thus, thrust vectoring performance remained similar to the 30° convergence angle case. However, the 40° convergence angle incurred the largest discharge coefficient penalties. The impact of cavity convergence angle on system thrust ratio, $C_{fg,sys}$, was relatively small. The effect of increasing cavity convergence angle on two flow details are apparent in Fig. 11, which shows the effect of cavity convergence angle on Mach contours; first, an upstream movement of an internal flow shock towards the sonic throat and, second, increased flow separation in the upper wall cavity.

D. Effect of Upstream Throat Height

It was hypothesized that increasing the upstream throat height (upstream throat area) might improve discharge coefficient while maintaining high levels of thrust vectoring efficiency by forcing a single throat area to occur at the nozzle exit. Obviously, the dual-throat concept becomes a single-throat (convergent nozzle) concept once the upstream minimum area is larger than the downstream minimum area. Figure 12, which presents the effect of throat height on Mach contours for 3% injection at NPR=4, indicates that sonic lines occur at both minimum areas for the h_{ut}=1.15 in. and 1.16 in. configurations. However for the h_{ut}=1.17 in. configuration, the sonic line at the upstream minimum mostly disappears while still occurring at the downstream minimum. Table 2 shows the effect of 0.01-inch increases in upstream throat height on thrust vectoring and nozzle performance. Unfortunately, the predicted results indicate that discharge coefficient does not improve as upstream minimum area increases. Additionally, thrust vectoring efficiency decreases slightly as the upstream minimum area increases. Simulations on upstream throat heights of 1.2 and 1.3 inches were also computed, but the unsteady flow in the cavity precluded predictions of converged nozzle performance.

	h_{ut}	h_{dt}	%-injection	$\delta_{p,}$ °	$\eta,$ °/%-injection	$C_{d,p}$	$C_{fg,sys}$
PAB3D	1.15	1.15	3.04	11.3	3.71	0.833	0.945
PAB3D	1.16	1.15	3.02	10.8	3.58	0.831	0.946
PAB3D	1.17	1.15	3.01	10.3	3.41	0.828	0.946

Table 2. Effect of throat height on nozzle performance for NPR=4 with 3% injection.

E. Effect of Pulsed Fluidic Injection

Typically, with both shock vector control and throat shifting methods, increasing the penetration of the secondary injected air increases the thrust vector angle generated from the accompanying increase in blockage of the primary exhaust flow. Although not shown in the current paper, the thrust vectoring capability of the DTN concept also increases with increased secondary injection. It is hypothesized that pulsed fluidic injection creates more blockage of the primary exhaust flow than steady injection and thus, yields greater thrust vector angles or, conversely, that less secondary fluidic injection is required with the pulsed system to get an equivalent thrust vector angle with steady injection, thus alleviating the engine performance penalty from bleeding air off the engine.

Increased penetration from pulsed secondary injection was demonstrated in a water-tunnel experiment at low speeds[34-36], but little research was found for pulsed injection into high-speed compressible flows. One recent computational investigation[37] of the effect of pulsed injection in a confined, expanding crossflow has looked at high-speed compressible flow conditions. The geometry for this investigation was a convergent duct, followed by a constant area section, with pulsed fluidic injection introduced at the beginning of the constant area section through a surface, square wave boundary condition.   It was deduced that the primary flow was near $M=1$ at the throat of the convergent geometry when operating at NPR=2. Results indicated that using an injection angle opposing the primary flow, and an optimum pulsing frequency produced gains in penetration and blockage compared to steady injection. No time average nozzle performance or thrust vector angles were calculated.

Unfortunately, results from the current computational investigation indicate no benefit of pulsed injection over steady injection for fluidic thrust vectoring using the Dual Throat Nozzle configuration at NPR=4. A large range of frequencies (2-100kHz), amplitudes (0.25, 0.5, 0.75) and duty cycles (25, 50, 75 percent) were investigated using a square wave boundary condition in an injection plenum. Representative results are show in Table 3. Discharge coefficient and primary thrust ratio were higher with the case shown in Table 3, but the time-averaged percent injection was also slightly higher than the steady injection case. System thrust ratio was not available as a time-averaged quantity for the pulsed injection case, which is why the comparison of primary thrust ratio ($F_r/F_{i,p}$) is made.

Pulsed injection did provide periodic improvement in secondary flow penetration into the primary exhaust flow when the square wave total pressure was at the peak level (Fig. 13(a)). However, the blockage of the primary flow was not maintained during the second half of the pulsing period when pressure was at a minimum (Fig. 13(b)). In the DTN configuration, the cavity depth provided relief of the vortex structures (Fig. 13(c)) developed from the pulsed injection, unlike the configuration in reference 37, where the constant area section provided no relief for the flow and the vortex structures were built up on top of each other. Therefore, the time averaged thrust vectoring efficiency for the DTN configuration was no better than using steady injection. For comparison, the vorticity magnitude contours for 4.9% steady injection at NPR=4 are shown in Fig. 14. Figure 15 shows total pressure contours as the high total pressure injects into the primary flow at the start of a new period (Fig. 15(a)), a vortex is shed into the primary flow (Fig. 15(b)), and finally the lower cavity wall is pressurized during the low total pressure portion of the pulsing period (Fig. 15(c)). Thrust vector angle is minimized when the lower cavity wall is pressurized, resulting in a time-averaged thrust vector efficiency less than that achieved with steady injection. For comparison, total pressure contours for 4.9% steady injection at NPR=4 are shown in Fig. 16. As a result of the pulsed injection computations, a planned experimental effort on pulsed injection on the DTN was deleted and the funds redirected to research on potentially more fruitful geometric studies such as cavity length that is reported in the companion paper[14].

Injection	%-injection	$\delta_{p,}$ °	$\eta,$ °/%-injection	$C_{d,p}$	$F_r/F_{i,p}$
Steady	4.9	9.97	2.02	0.861	0.971
10kHz Pulsed	5.4	9.65	1.80	0.875	0.979

Table 3. Comparison of nozzle performance for steady and pulsed injection at NPR=4.

IV.   Conclusions

The NASA Langley developed, fluidic thrust vectoring, Dual Throat Nozzle has achieved levels of thrust vectoring efficiency greater than any other fluidic thrust vectoring concept reported in the open literature. In

addition, the Dual Throat Nozzle technique does not compromise system thrust ratio, unlike shock vector control methods that incur large thrust penalties with the creation of the shock required for turning. The design of the fluidic thrust vectoring, Dual Throat Nozzle was guided with the aid of the computational method PAB3D and the concept has been successfully demonstrated experimentally in the NASA Langley Research Center Jet Exit Test Facility. For example, at a nozzle pressure ratio of 4, experimental thrust vectoring efficiency was 6.1 degrees/percent injection with 1 percent injection and thrust ratio was 0.968, which was only 0.5 percent loss compared to non-vectoring case. However, additional development is probably required to alleviate or compensate for lower than desired discharge coefficients.

Computational results indicate that increasing cavity divergence angle beyond 10° is detrimental to thrust vectoring efficiency, while increasing cavity convergence angle from 20° to 30° improves thrust vectoring efficiency, albeit at the expense of discharge coefficient. Increasing cavity divergence angle caused a 2% penalty in system thrust ratio with little effect on discharge coefficient, while the reciprocal was true for cavity convergence angle. Increasing cavity convergence angle had little impact on system thrust ratio, while decreasing discharge coefficient up to 3%.

Several pulsed injection variables were investigated computationally and the results indicate that pulsed fluidic injection on the Dual Throat Nozzle concept was no more effective for thrust vectoring than steady fluidic injection. Pulsed fluidic injection did increase penetration of the secondary air stream, as indicated for a convergent configuration found in literature. However, the recessed cavity in the Dual Throat Nozzle provides relief for the flow and the vortex structures break down in the cavity instead of building up on each other to maintain primary flow blockage. Thus, the time averaged thrust vector angle with pulsed injection was no better than steady injection.

In evaluating absolute magnitude of nozzle performance and thrust vector angles, PAB3D inaccurately predicted pressure losses that occur in the large regions of separated flow of the cavity, which is not completely unexpected from most computational flow solvers. An important result from this work is that PAB3D can predict the trends of thrust vectoring efficiency, discharge coefficient and system thrust ratio for a variety of geometric and flow condition variables. Thus, PAB3D is an invaluable tool for screening a plethora of variables, without the expense of model fabrication and facility test time. From the current work, substantial funds were saved and redirected from experimentally investigating pulsed injection techniques, towards investigating other promising geometric variations of the Dual Throat Nozzle concept.

References

[1]Anderson, C. J.; Giuliano, V. J.; and Wing, David J.: Investigation of Hybrid Fluidic / Mechanical Thrust Vectoring for Fixed-Exit Exhaust Nozzles. AIAA 97-3148, July 1997.

[2]Giuliano, V. J.; and Wing, David J.: Static Investigation of a Fixed-Aperture Exhaust Nozzle Employing Fluidic Injection for Multiaxis Thrust Vector Control. AIAA 97-3149, July 1997.

[3]Waithe, Kenrick A.: An Experimental and Computational Investigation of Multiple Injection Ports in a Convergent-Divergent Nozzle for Fluidic Thrust Vectoring. Master of Science Thesis, May 2001.

[4]Deere, K. A.: Computational Investigation of the Aerodynamic Effects on Fluidic Thrust Vectoring. AIAA 2000-3598, July 2000.

[5]Wing, David J.: Static Investigation of Two Fluidic Thrust-Vectoring Concepts on a Two-Dimensional Convergent-Divergent Nozzle. NASA TM-4574, December 1994.

[6]Wing, David J.; and Giuliano, V. J.: Fluidic Thrust Vectoring of an Axisymmetric Exhaust Nozzle at Static Conditions. ASME FEDSM97-3228, June 1997.

[7]Deere, Karen A.; and Wing, David J.: PAB3D Simulations of a Nozzle with Fluidic Injection for Yaw-Thrust-Vector Control. AIAA 98-3254, July 1998.

[8]Miller, D. N.; Yagle, P. J.; and Hamstra, J. W.: Fluidic Throat Skewing for Thrust Vectoring in Fixed Geometry Nozzles. AIAA 99-0365, January 1999.

[9]Yagle, P. J.; Miller, D. N.; Ginn, K. B.; and Hamstra, J. W.: Demonstration of Fluidic Throat Skewing for Thrust Vectoring in Structurally Fixed Nozzles. 2000-GT-0013, May 8-11, 2000.

[10]Deere, K. A.; Berrier, B. L.; Flamm, J. D.; and Johnson, S. K.: Computational Study of Fluidic Thrust Vectoring Using Separation Control in a Nozzle. AIAA-2003-3803, June 2003.

[11]Hunter, C.A.; and Deere, K. A.: Computational Investigation of Fluidic Counterflow Thrust Vectoring. AIAA 99-2669, June 1999.

[12]Flamm, J. D.: Experimental Study of a Nozzle Using Fluidic Counterflow for Thrust Vectoring. AIAA 98-3255, July 1998.

[13]Deere, K. A.: Summary of Fluidic Thrust Vectoring Research Conducted at NASA Langley Research Center. AIAA-2003-3800, June 2003.

[14]Flamm, J. D.; Berrier, B. L.; Johnson, S. K.; and Deere, K. A.: An Experimental Study of a Dual Throat Fluidic Thrust Vectoring Nozzle Concept. AIAA-2005-3503, July 2005.

[15]Abdol-Hamid, K. S.: The Application of 3D Marching Scheme for the Prediction of Supersonic Free Jets. AIAA 89-2897. July 1989.

[16]Abdol-Hamid, K. S.: Application of a Multiblock/ Multizone Code (PAB3D) for the Three-Dimensional Navier-Stokes Equations. AIAA-91-2155, June 1991.

[17]Carlson, J. R.: A Nozzle Internal Performance Prediction Method. NASA TP 3221, October 1992.

[18]Carlson, J. R.: Computational Prediction of Isolated Performance of an Axisymmetric Nozzle at Mach Number 0.90. NASA TM 4506, February 1994.

[19]Pao, S. P., Carlson, J. R., and Abdol-Hamid, K. S.: Computational Investigation of Circular-to-Rectangular Transition Ducts. Journal of Propulsion and Power, Vol. 10, No. 1, p 95-100, Jan.-Feb. 1994.

[20]Abdol-Hamid, K. S.; Lakshmanan, B.; and Carlson, J. R.: Application of Navier-Stokes Code PAB3D With k-e Turbulence Model to Attached and Separated Flows. NASA TP-3480, January 1995.

[21]Abdol-Hamid, K. S., Carlson, J. R., and Pao, S. P.: Calculation of Turbulent Flows Using Mesh Sequencing and Conservative Patch Algorithm. AIAA 95-2336, July 1995.

[22]Pao, S. P.; and Abdol-Hamid, K. S.: Numerical Simulation of Jet Aerodynamics Using the Three-Dimensional Navier-Stokes Code PAB3D. NASA TP 3596, September 1996.

[23]Abdol-Hamid, K. S.; Lakshmanan, B.; and Carlson, J. R.: Application of Navier-Stokes Code PAB3D With k-e Turbulence Model to Attached and Separated Flows. NASA TP-3480, January 1995.

[24] Carlson, J. R.: Applications of Algebraic Reynolds Stress Turbulence Models Part 1: Incompressible Flat Plate. Journal of Propulsion and Power, Vol. 13, No. 5, p 610-619, Sept.-Oct. 1997.

[25]Abdol-Hamid, K., Pao, S., Massey, S., and Elmiligui, A.: Temperature Corrected Turbulence Model for High Temperature Jet Flow. ASME Journal of Fluids Engineering, Vol. 126, No. 5, September 2004.

[26]Balakrishnan, L.; and Abdol-Hamid, K. S.: A Comparative Study of Two Codes with an Improved Two-Equation Turbulence Model For Predicting Jet Plumes. AIAA 92-2604, June 1992.

[27]Girimaji, S. S.: Fully-Explicit and Self-Consistent Algebraic Reynolds Stress Model. Inst. For Computer Applications in Science and Engineering, 95-82, December1995.

[28]Abdol-Hamid, K. S.: Implementation of Algebraic Stress Models in a General 3-D Navier-Stokes Method (PAB3D). NASA CR-4702, 1995.

[29]Abdol-Hamid, K. S. and Girimaji, S. S.: A Two-Stage Procedure Toward the Efficient Implementation of PANS and Other Hybrid Turbulence Models. NASA/TM-2004-213260, August 2004.

[30]Massey, S. J.; and Abdol-Hamid, K. S.: Enhancement and Validation of PAB3D for Unsteady Aerodynamics. AIAA 2003-1235, January 2003.

[31]Elmiligui, A., Abdol-Hamid, K., and Hunter, C.: Numerical Investigation of Flow in an Over-expanded Nozzle with Porous Surfaces. AIAA 2005-4159, July 2005.

[32]van Leer, B.: Flux-Vector Splitting for the Euler Equations. ICASE Report 82-30, 1982.

[33]Jones, W. P.; and Launder, B. E.: The Prediction of Laminarization With a Two-Equation Model of Turbulence. Int. Journal of Heat & Mass Transfer, vol. 15, no. 2, February 1972, pp. 301-314.

[34]Vakili, A. D., Chang, Y. K., and Wu, J. M.: Vortex Rings in Uniform Crossflow. AIAA Paper 91-0552, 1991.

[35]Vakili, A. D., Sauerwein, S., and Miller, D. N.: Pulsed Injection Applied to Nozzle Internal Flow Control. AIAA 99-1002, 1999.

[36]Eroglu, A. and Breidenthal, R. E.: Effects of Periodic Disturbances on Structure and Flame Length of a Jet in a Crossflow. AIAA Paper 91-0317, 1991.

[37]Miller, D. N.; Yagle, P. J.; Bender, E. E., Smith, B. R., and Vermeulen, P. J.: A computational Investigation of Pulsed Injection Into a Confined, Expanding Crossflow. AIAA 2001-3026, June 2001.
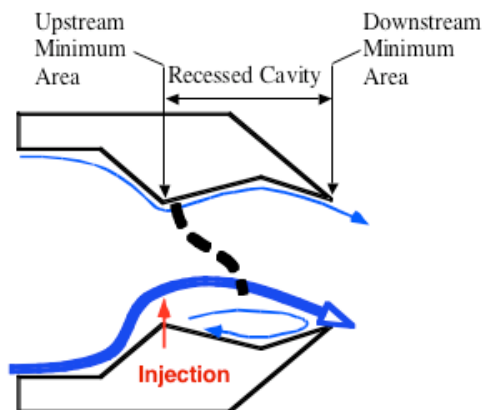
Figure 1. Sketch of the Dual Throat Nozzle Concept with fluidic injection at the upstream minimum area.
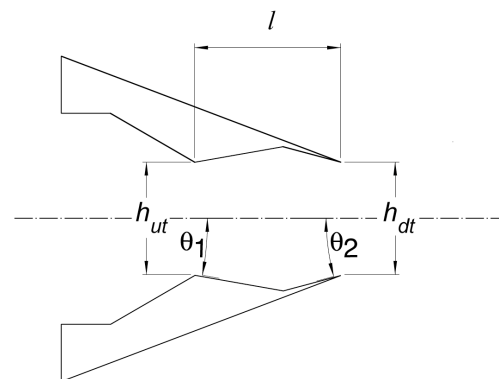
Figure 2. Sketch of the design variables for the Dual Throat Nozzle.
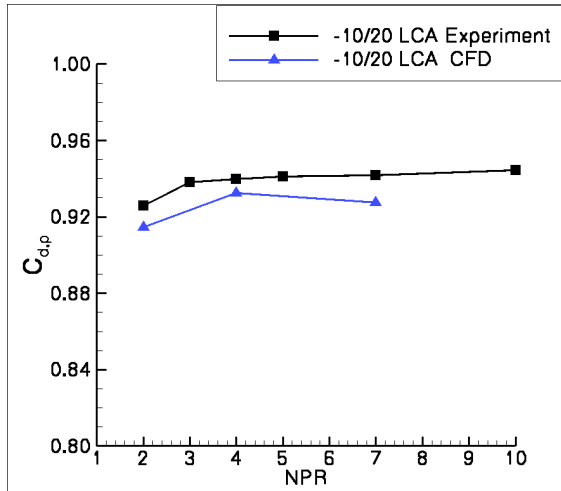
(a)   Discharge coefficient, No Injection
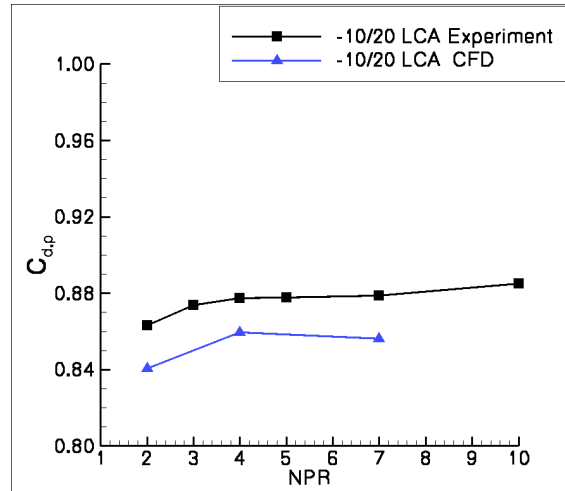
(d) Discharge coefficient, 3% Injection
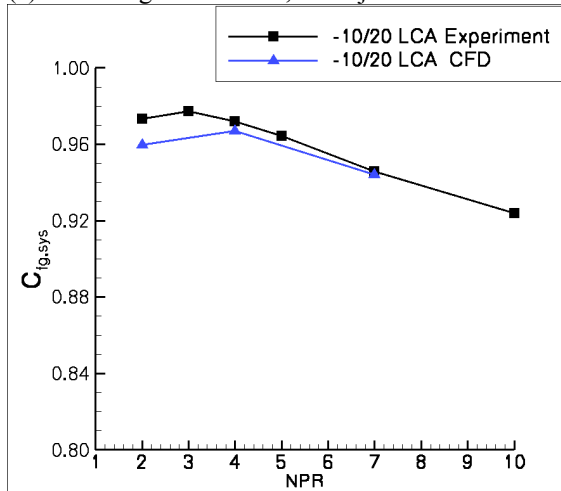
(b) System thrust ratio, No Injection
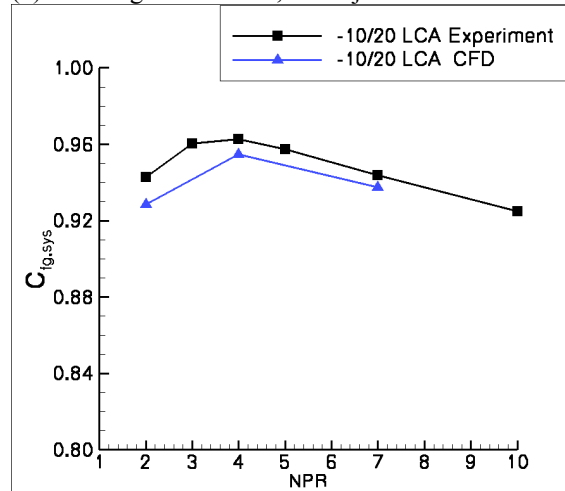
(e) System thrust ratio, 3% Injection
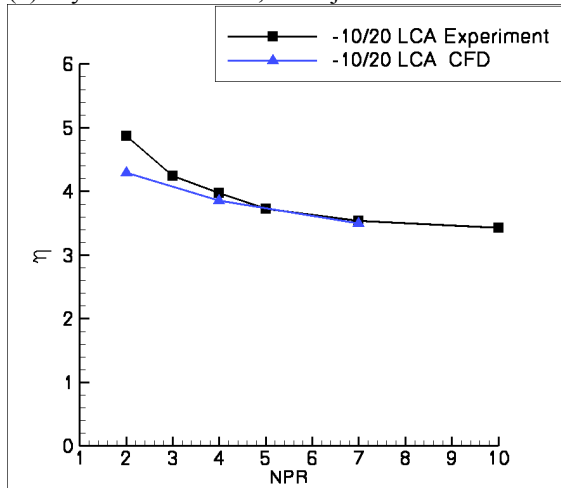
(c)   Thrust vectoring efficiency, 3% Injection
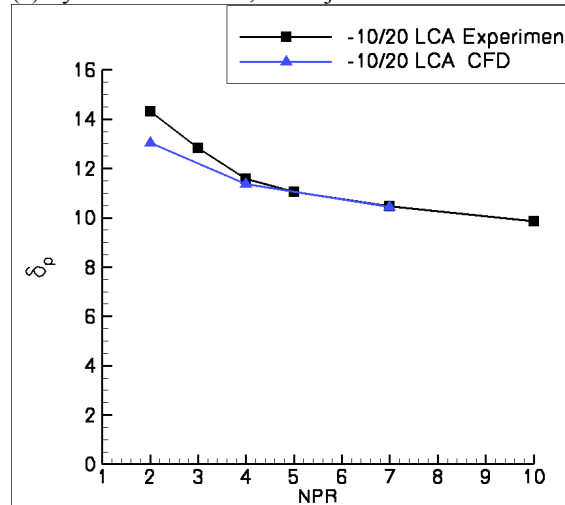
(f) Thrust vector angle, 3% Injection

Figure 3.   Comparison of experimental and computational thrust vectoring and nozzle performance, configuration 1.

11
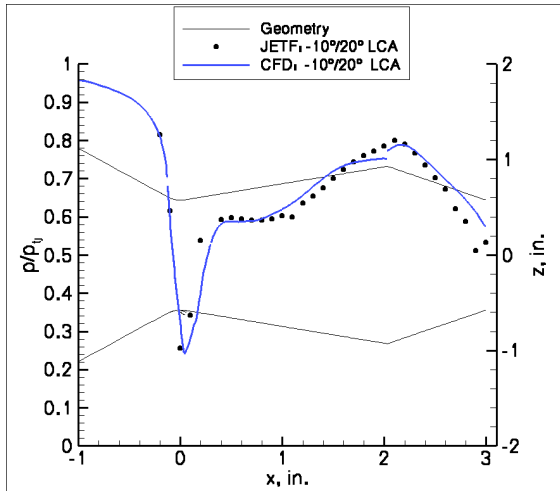
(a) Upper-wall normalized pressure distributions.
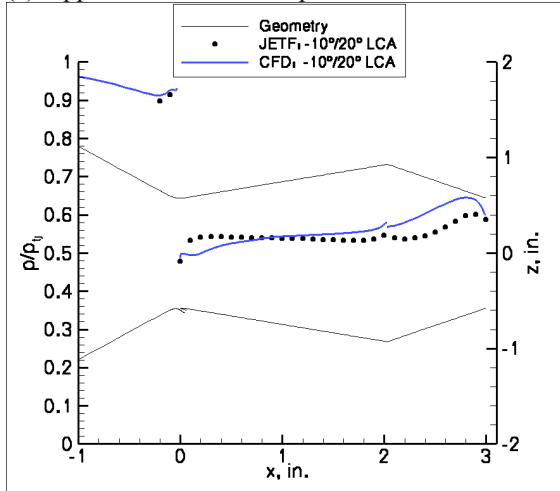
(b) Lower-wall normalized pressure distributions.

Figure 4. Comparison of predicted and experimental data at NPR=2, 3% injection.
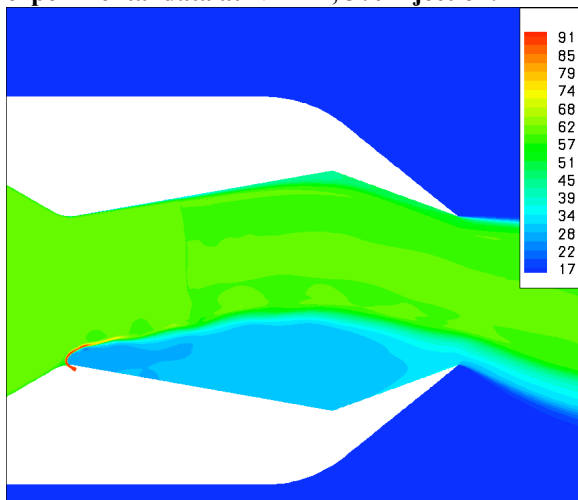
Figure 5. Total pressure contours (psi) for configuration 1 at NPR=4, 3% injection.
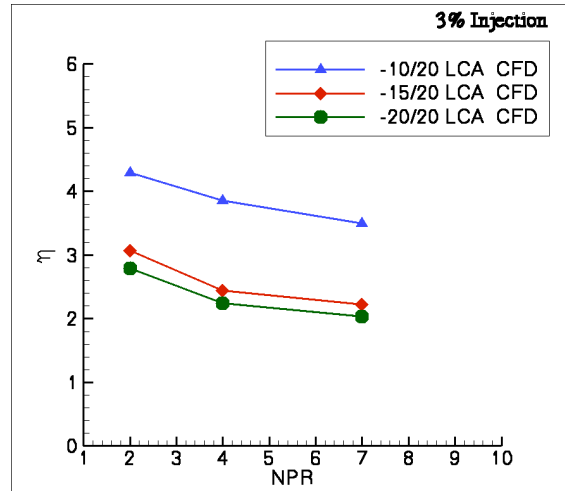
(a) Thrust vectoring efficiency
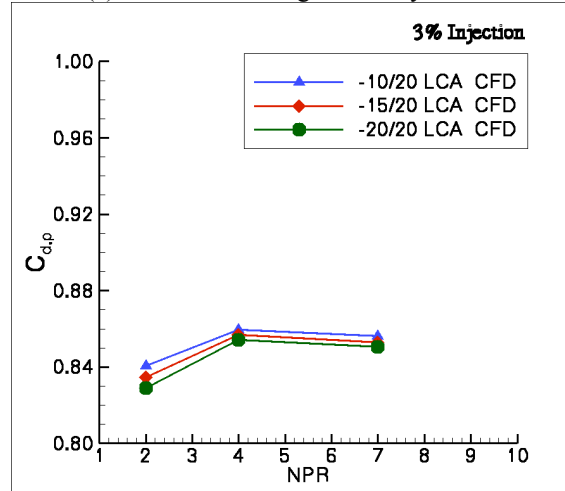
(b) Discharge coefficient
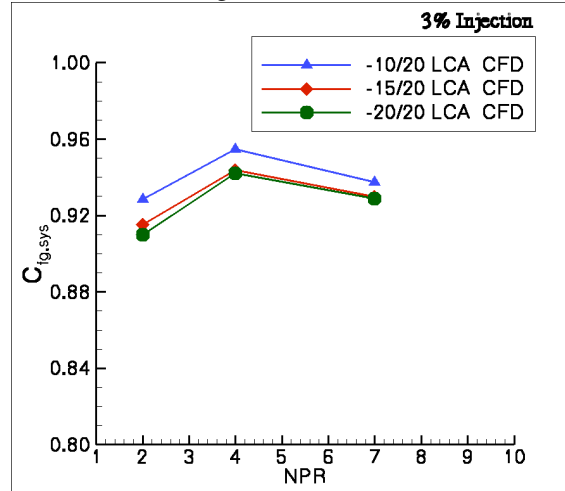
(c) System thrust ratio

Figure 6. Effects of divergence angle on thrust vectoring and nozzle performance.

12

American Institute of Aeronautics and Astronautics
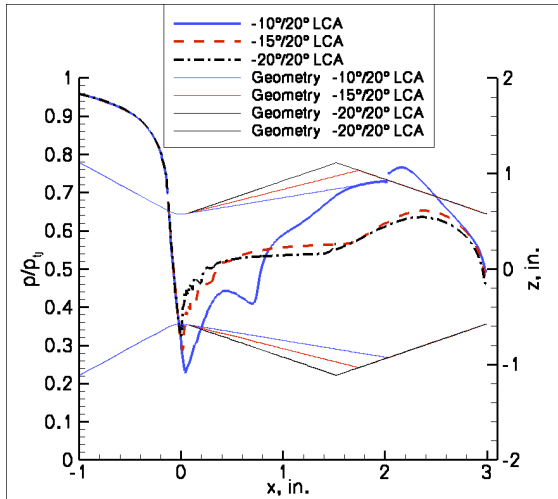
(a)   Pressures along the upper wall.

(b)   Pressures along the lower wall.

Figure 7.   Effect of cavity divergence angle on normalized wall pressures, NPR=4, 3% injection.
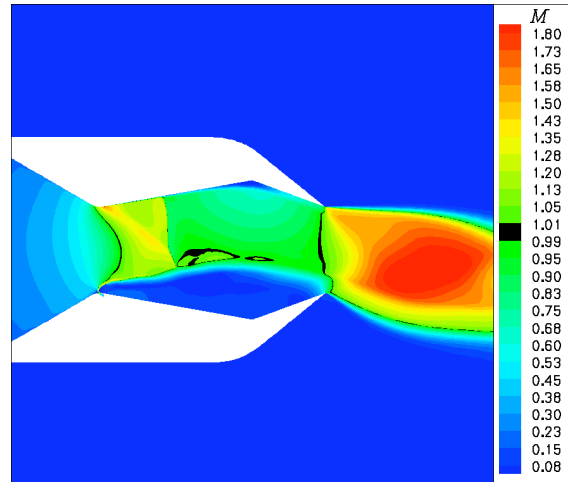

(a)   10° Cavity Divergence Angle
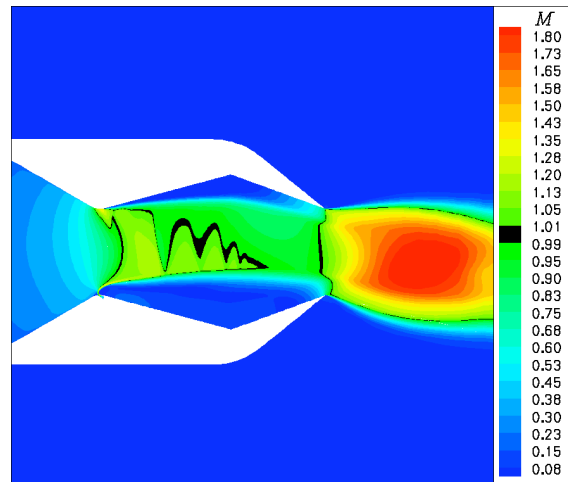
(b)   15° Cavity Divergence Angle
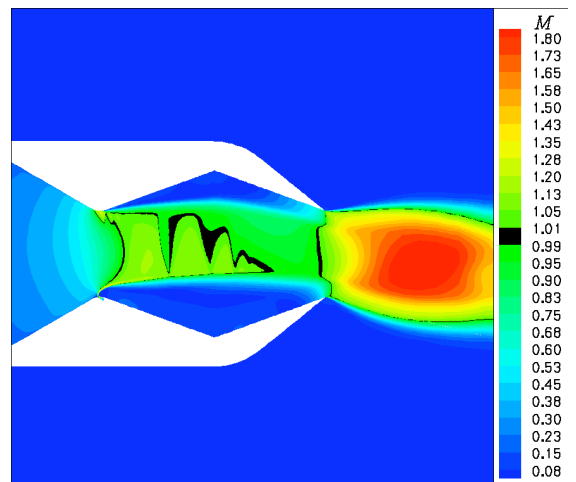
(c)   20° Cavity Divergence Angle

Figure 8.   Effect of cavity divergence angle on Mach contours, NPR=4, 3% injection.
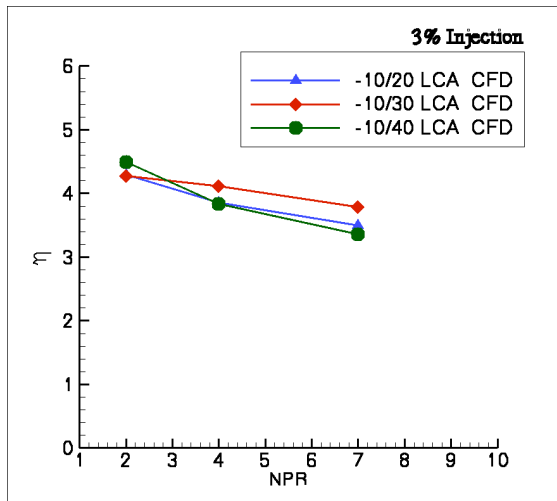
(a) Thrust vectoring efficiency
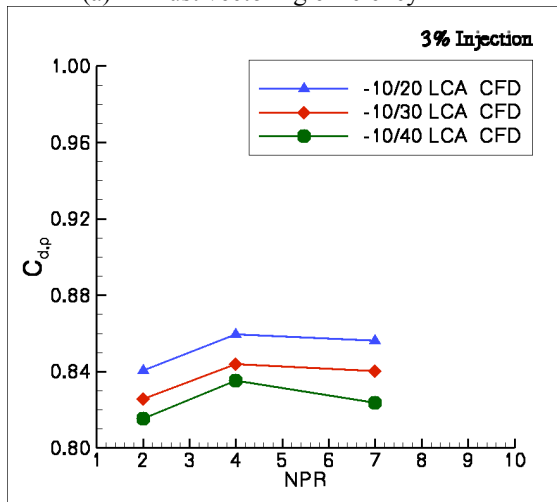
(b) Discharge coefficient
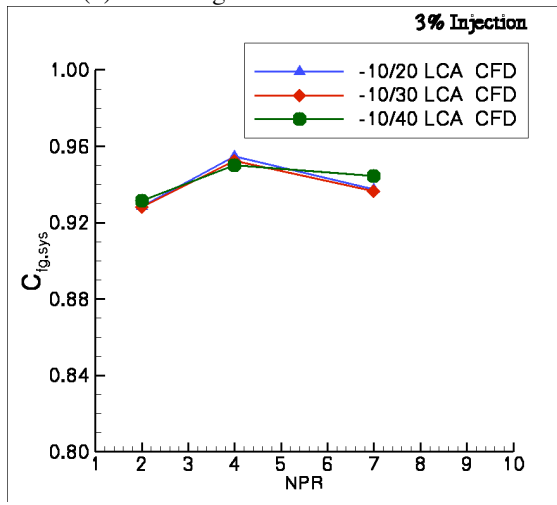
(c) System thrust ratio

Figure 9.   Effect of convergence angle on thrust vectoring and nozzle performance.
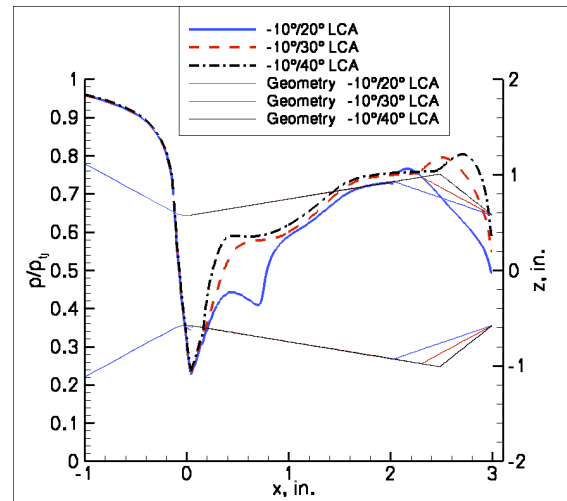
(a) Pressures along the upper wall.
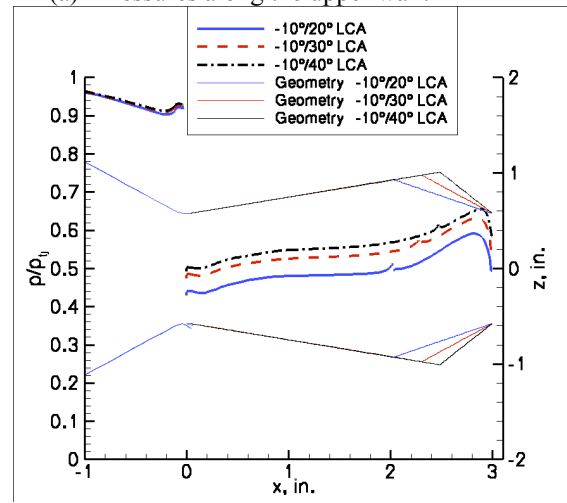
(b) Pressures along the lower wall.

Figure 10.   Effect of cavity convergence angle on normalized wall pressures, NPR=4, 3% injection.

American Institute of Aeronautics and Astronautics
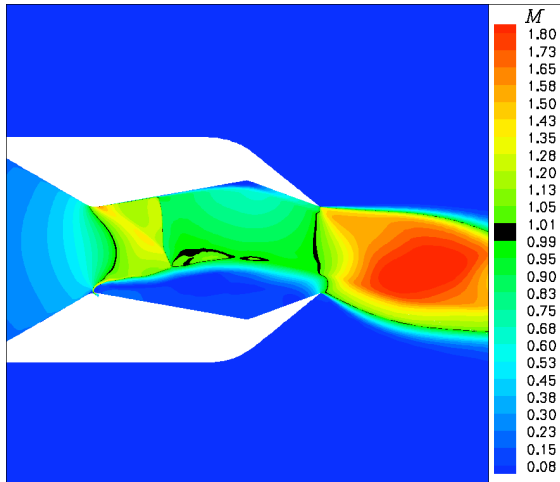
(a) 20° cavity convergence angle
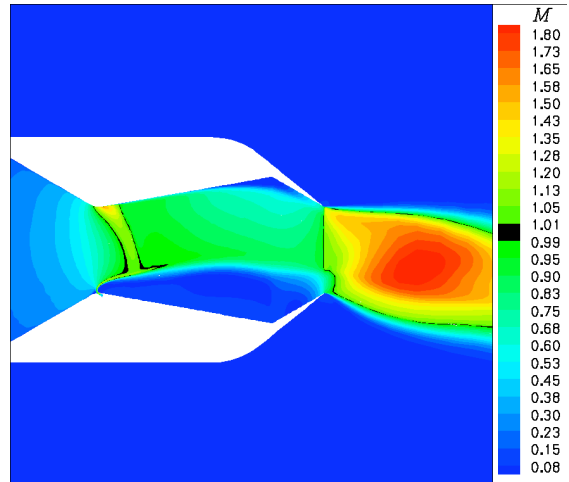
a) h_{ut}=1.15 inches
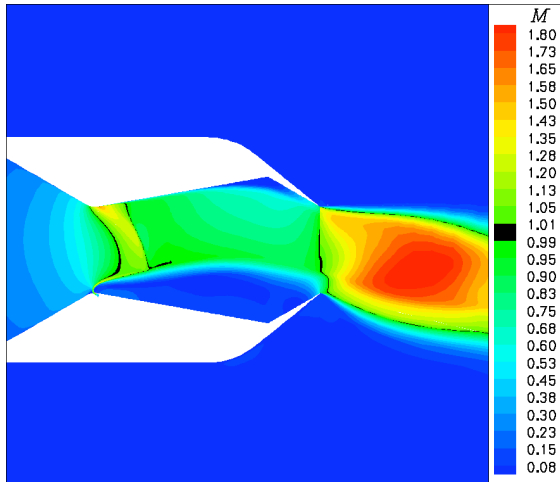
(b) 30° cavity convergence angle
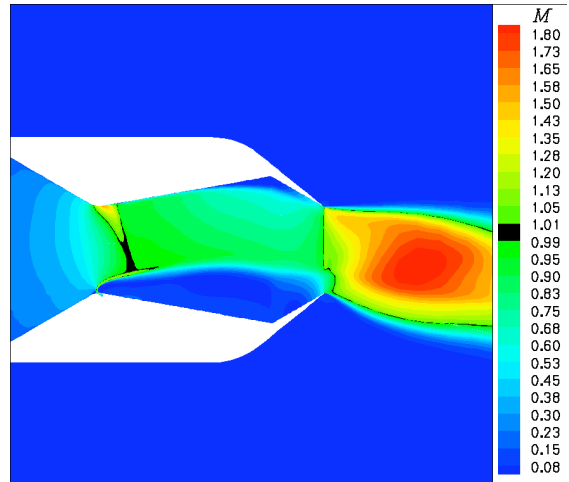
b) h_{ut}=1.16 inches
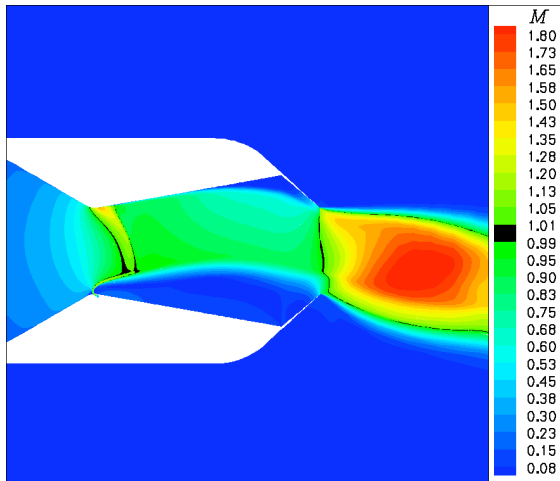
(c) 40° cavity convergence angle
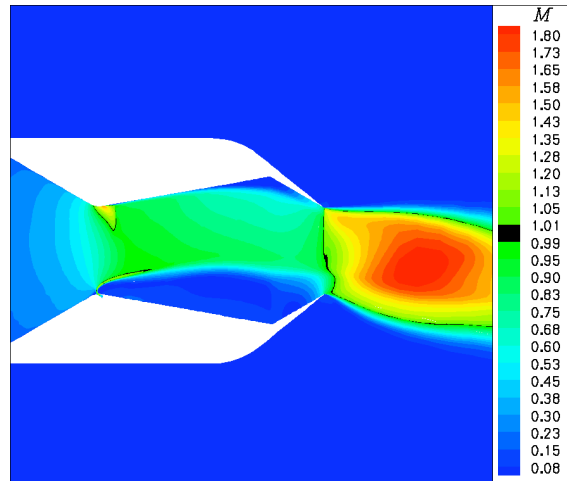
Figure 11. Effect of cavity convergence angle on Mach contours, NPR=4, 3% injection.

c) h_{ut}=1.17 inches

Figure 12. Effect of upstream throat height on Mach contours, NPR=4, 3% injection.
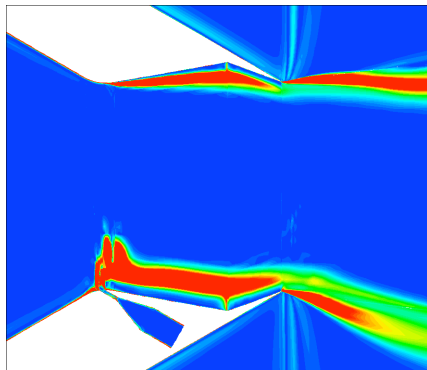
(a) Peak penetration
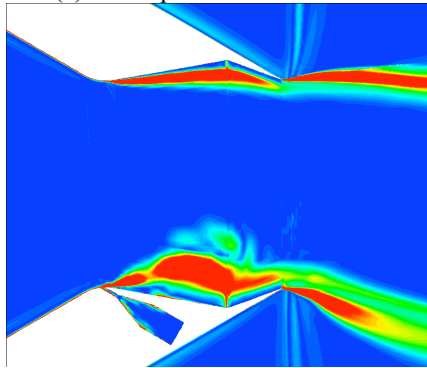
(b) Minimum penetration
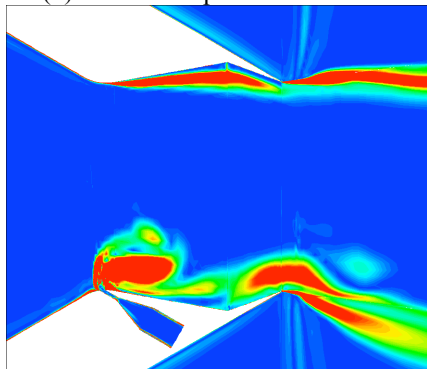
(c) Start of next period

Figure 13. Vorticity magnitude contours NPR=4, 10kHz square wave pulsing frequency.
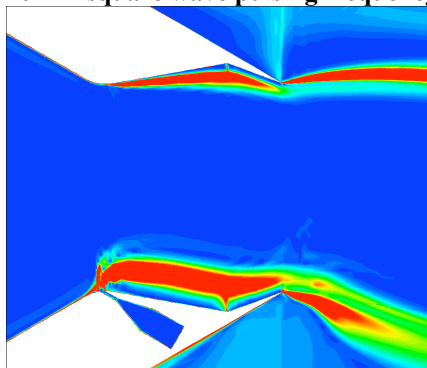

Figure 14. Vorticity magnitude contours NPR=4, 4.9% steady injection.
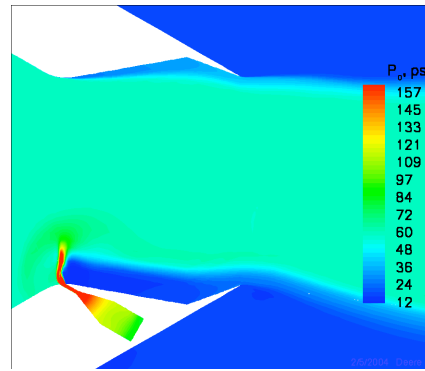
a)   Peak penetration with high total pressure
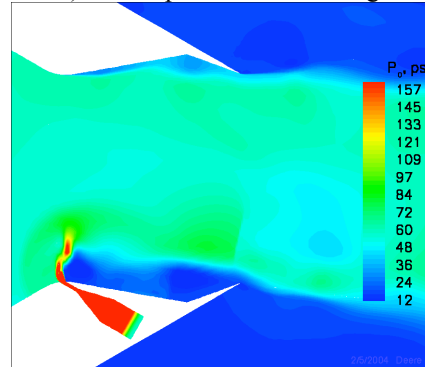
b)   Vortex shed and moves downstream
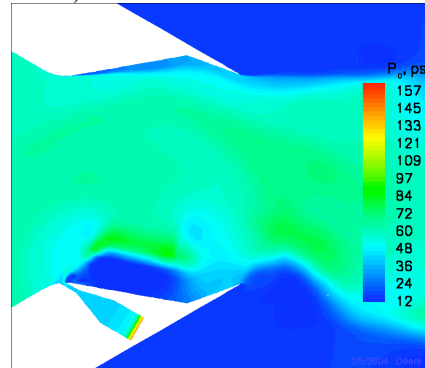
c)   Vector angle decreases as flow pressurizes the lower converging cavity wall.

Figure 15.   Total pressure contours for pulsed injection case, 10kHz frequency, at NPR=4.
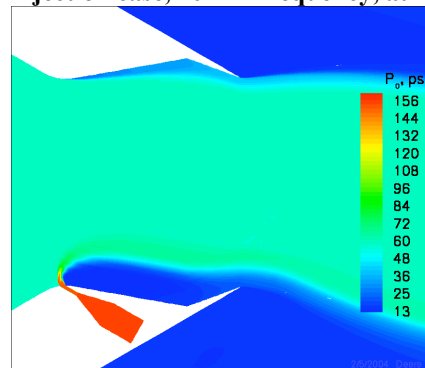

Figure 16.   Total pressure contours for 4.9% steady injection at NPR=4.